Work-Function Engineering of Graphene Anode by Bis(trifluoromethanesulfonyl)amide Doping for Efficient Polymer Light-Emitting Diodes

*Donghyuk Kim, Dongchan Lee, Yonghee Lee, and Duk Young Jeon**

Graphene has been considered to be a potential alternative transparent and flexible electrode for replacing commercially available indium tin oxide (ITO) anode. However, the relatively high sheet resistance and low work function of graphene compared with ITO limit the application of graphene as an anode for organic or polymer light-emitting diodes (OLEDs or PLEDs). Here, flexible PLEDs made by using bis(trifluoromethanesulfonyl)amide (TFSA, $[CF_3SO_2]_2NH$) doped graphene anodes are demonstrated to have low sheet resistance and high work function. The graphene is easily doped with TFSA by means of a simple spin-coating process. After TFSA doping, the sheet resistance of the TFSA-doped five-layer graphene, with optical transmittance of ≈88%, is as low as ≈90 Ω sq^{-1}. The maximum current efficiency and power efficiency of the PLED fabricated on the TFSA-doped graphene anode are 9.6 cd A^{-1} and 10.5 lm W^{-1}, respectively; these values are markedly higher than those of the PLED fabricated on pristine graphene anode and comparable to those of an ITO anode.

1. Introduction

As graphene can be successfully detached from graphite and transferred onto another substrate it has attracted great attention, also due to its superb electronic, optical, and mechanical properties.[1] Graphene has been considered to be a potential alternative transparent electrode because of its high transparency and low sheet resistance.[2–4] Graphene is a two-dimensional flexible sheet consisting of sp^2-hybridized carbon atoms and can replace conventional brittle indium tin oxide (ITO) electrodes in flexible devices such as electroluminescent devices,[5] organic light-emitting diodes (OLED),[6] photovoltaics,[7–9] and light-emitting electrochemical cells.[10]

Despite the aforementioned advantages as a transparent electrode, graphene has limitations as an anode material for organic or polymer light-emitting diode (OLED or PLED) due to its relatively high sheet resistance and low work function compared with ITO, which is conventionally used as an anode. The low work function of graphene causes inefficient hole injection from the graphene anode to the hole-transporting layer (HTL) due to an increased potential barrier between graphene and HTL. Consequently, the efficiency of OLEDs fabricated on the graphene anode becomes poorer than those of OLEDs fabricated on ITO anode. To decrease sheet resistance of graphene and tune its work function, it has been doped by various methods such as electrical gating,[11,12] and substitutional[13–15] and chemical doping.[16–18] Among those methods, electrical gating is undesirable for the application as an anode because it requires bias voltages for operation. In the case of substitutional doping, application of bias voltage is not needed. However, the process of substituting carbon atoms in the basal plane of graphene is relatively complicated.[19] Chemical doping has been developed as it has some advantages such as a facile doping process and an ease of finding dopants. Chemical doping is easily achieved by using spin- or dip-coated chemical species, including various acids, metal chlorides, and other molecules.[20–25]

Bis(trifluoromethanesulfonyl)amide (TFSA, $CF_3SO_2]_2NH$) has been reported as a strong p-type chemical dopant for carbon nanotubes and graphene due to the presence of a strong electron-withdrawing group.[26–28] As a p-type chemical dopant of graphene for anodes of PLEDs, TFSA has some advantages such as effective electron-withdrawing ability, maintaining high transmittance, smooth surface, and stability.[27] Our approach is to apply chemically doped graphene to the anode of a PLED. Our graphene samples were chemically doped by using spin-coated TFSA and PLEDs were fabricated on the doped graphene by a spin-coating process. The sheet resistance of our samples was reduced and their work function increased after chemical doping by using TFSA. Efficient hole injection from the doped graphene anode to HTL occurs due to decrease of potential barrier between the graphene anode and HTL. Consequently, efficiency of the PLED was improved by introduction of the TFSA-doped graphene anode. The decrease of hole-injection barrier from the TFSA-doped graphene anode to HTL in the PLED results in marked enhancement of device performance that is comparable to that of the device fabricated on a commercially used ITO anode.

D. Kim, D. Lee, Y. Lee, Prof. D. Y. Jeon
Department of Materials Science and Engineering
KAIST, 291 Daehak-ro, Yuseong-gu
Daejeon, 305–701, Republic of Korea
E-mail: dyj@kaist.ac.kr

DOI: 10.1002/adfm201301386

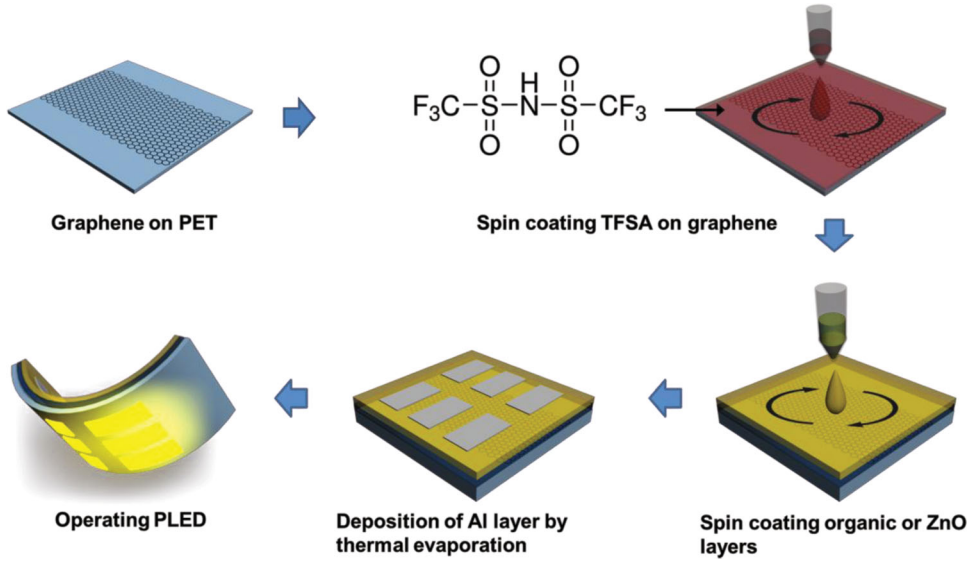

Figure 1. Schematics of a synthesis of TFSA-doped graphene samples and a fabrication procedure of the flexible PLED built on the TFSA-doped graphene/PET substrate.

2. Results and Discussion

Figure 1 illustrates the procedure for a synthesis of doped graphene samples by using TFSA and the fabrication procedure of the flexible PLED built on the TFSA-doped graphene/polyethylene terephthalate (PET) substrate. The graphene samples were grown on copper foils by using a CVD apparatus with methanol as carbon source. After growth, the graphene on the copper foil was transferred onto an arbitrary substrate such as a PET or a SiO_2 wafer. by dry transfer.[4] To form multilayered graphene on an arbitrary substrate, this process was repeated until the desired number of graphene layers was obtained. The graphene on the substrate was easily chemically doped by spin-coating TFSA dissolved in nitromethane onto the graphene. After synthesis and TFSA-doping, a flexible PLED was fabricated on the flexible and transparent TFSA-doped graphene anode by a spin-coating process. Poly(3,4-ethylenedioxythiophene):poly(styrenesulfonate) (PEDOT:PSS) and Super Yellow–PPV (SY) layers were spin-coated onto the TFSA-doped graphene/PET substrate. The ZnO nanoparticle layer and, immediately after, ionic solution (a blend of polyethylene oxide [PEO] and tetra-n-butylammonium tetrafluoborate [$TBABF_4$]) were spin-coated and subsequently aluminum layers were thermally evaporated onto the polymer layers.

Figure 2a shows the transmittance of the graphene samples with varied numbers of graphene layers by dry transfer. The transmittance of one- to five-layer pristine graphene samples was 97.5%, 95.0%, 92.9%, 90.0%, and 87.9%, respectively. Usually, transmittance of graphene decreases by ≈2.2%–2.3% with each added layer, which implies that the average thickness of sample per dry-transfer process is approximately a monolayer.[4] Electrical properties of the graphene samples were also investigated. Sheet resistance values of one- to five-layer pristine graphene samples were 5590, 1050, 660, 460, and 240 Ω sq^{-1}, respectively. As the number of layers increased, the transmittance and the sheet resistance decreased. After TFSA doping, the sheet resistance of one- to five-layer graphene samples were 2340, 420, 230, 170, and 90 Ω sq^{-1}, respectively (Figure 2b). Graphene can be easily doped due to its unique electronic band structure.[4] TFSA has a strong electron-withdrawing group, which induces local charge from adjacent materials.[26,27] Reduction of the sheet resistance can be attributed to increase of hole carriers due to induced local charge by TFSA.

The sheet resistance of the TFSA-doped graphene decreased with increasing concentration of TFSA. Depending on the concentration of TFSA, the sheet resistance decreased by ≈65% with an increase in concentration of TFSA up to 15 mM. Increasing the concentration of TFSA beyond 15 mM no longer affected the sheet resistance (Figure 2c,d). After TFSA doping, there was no significant change in the transmittance. It is known that visible light is not absorbed by TFSA,[26] therefore, the decrease in the transmittance of TFSA-doped graphene was negligible compared with the transmittance of the pristine graphene. This negligibly decreased transmittance is one of the advantages of adopting TFSA as a dopant. TFSA doping improved the conductivity; the sheet resistance of the TFSA-doped five-layer graphene with optical transmittance of ≈88% was as low as ≈90 Ω sq^{-1}.

Raman spectroscopy is a nondestructive and powerful tool to determine the number of graphene layers and quality of the graphene.[29] **Figure 3**a shows the Raman spectra of the pristine graphene and TFSA-doped graphene with the number of graphene layer. For all the samples, the Raman spectra show typical features of the graphene. Three peaks were observed at ≈1350, ≈1595, and ≈2700 cm^{-1} that correspond to the defect-related D peak, G peak, and 2D peak, respectively. The intensity ratio of the 2D to G peak of the pristine graphene decreased with an increasing number of graphene layers. Raman spectra are affected by doping and the peak shift indicates that the graphene was successfully doped.[11,16,27] After TFSA doping, the G peak and 2D peak in the Raman spectrum were shifted compared with for the pristine graphene. The G peak and 2D peak

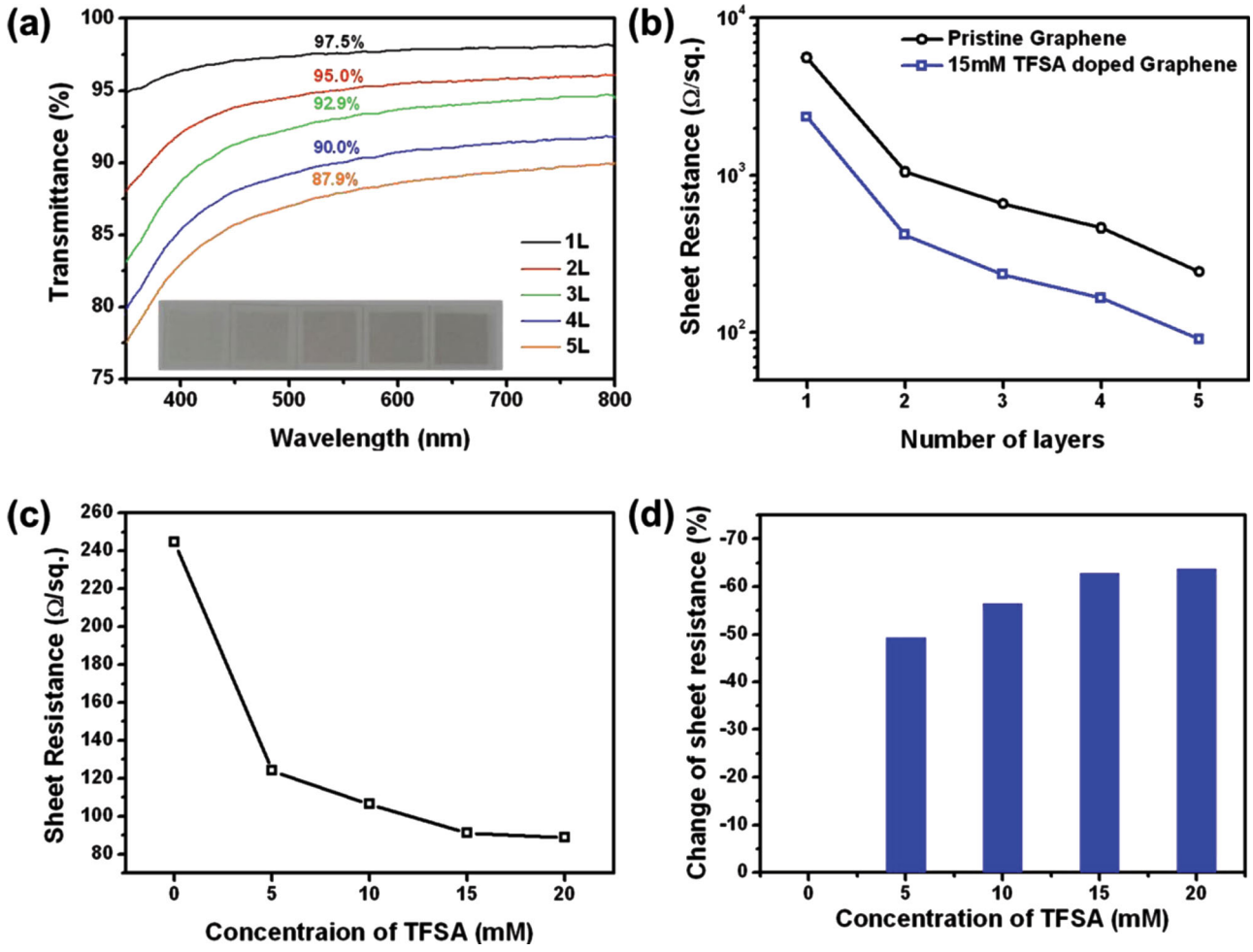

Figure 2. a) Transmittance spectra of pristine graphene with number of layers. b) Sheet resistance of pristine and TFSA-doped graphene samples with number of layers. c) Sheet resistance of TFSA-doped graphene samples with various concentrations of TFSA. d) Change of sheet resistance with concentration of TFSA.

shifted with increasing concentration of TFSA. The G peak started at 1587 cm^{-1} and shifted up to 1611 cm^{-1}, while the 2D peak started at 2691 cm^{-1} and was shifted up to 2707 cm^{-1}. Increasing the concentration of TFSA beyond 15 mM no longer affected the peak shift (Figure 3b,c). This result agrees well with that of the sheet resistance of TFSA-doped graphene; the sheet resistance and the Raman peak shift of TFSA-doped graphene were saturated at 15 mM TFSA.

An important factor to consider for anode application in PLEDs is surface roughness. The surface of the anode should be smooth to avoid a short circuit between anode and cathode. **Figure 4** shows AFM images and line profiles of pristine graphene, $AuCl_3$-doped graphene, and TFSA-doped graphene. The surface of the pristine graphene was smooth, with a root-mean-square (RMS) value of 3 nm, as shown in Figure 4a and b. After $AuCl_3$ doping, gold particles with a size distribution of 30–120 nm were observed on the graphene (Figure 4c,d). $AuCl_3$ is a well-known effective p-type dopant for graphene, however, gold particles on top of the surface of the graphene anode cause short circuit and increased leakage current in the devices.[6,29] On the other hand, the surface of TFSA-doped graphene was also smooth and protrusion was not observed as shown in Figure 4e and f, where the RMS value fluctuates little, which is reasonably good for anode application in PLEDs.

To investigate the performance of PLEDs based on TFSA-doped graphene anodes, the TFSA-doped graphene film transferred onto a PET substrate was applied as a flexible and transparent electrode for the PLED. **Figure 5**a illustrates the device structure of a flexible PLED fabricated on graphene. The device characterization of the PLEDs is presented in **Table 1** in terms of the current density versus applied voltage, luminance versus applied voltage, and the current efficiency versus voltage, as shown in Figure 5b–d. The performance of the PLED improved after TFSA doping. The PLED on five-layer graphene doped with 15 mM TFSA exhibited the highest luminance of 5400 cd m^{-2} at 6.0 V, highest current efficiency of 9.6 cd A^{-1} at 3.6 V, and highest power efficiency of 10.5 lm W^{-1} at 2.6 V. When the TFSA-doped graphene was applied as the anode, maximum luminance, maximum current efficiency, and maximum power efficiency were enhanced by 230%, 160%, and 200%, respectively. These results are comparable to those obtained for the PLED fabricated on an ITO anode and those reported in other references.[30]

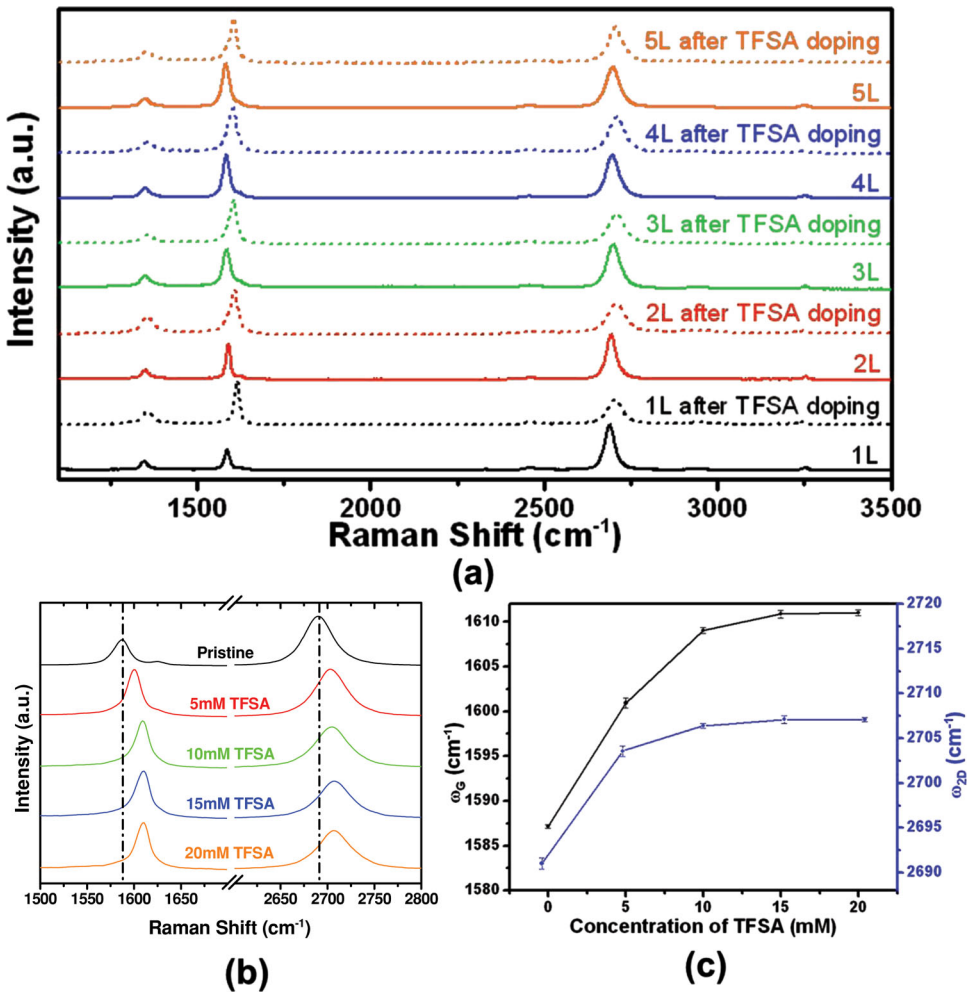

Figure 3. a) Raman spectra of pristine and 15 mM TFSA-doped graphene with number of layers. b) Raman spectra of graphene with concentration of TFSA. c) Raman peak position of G and 2D peak of TFSA-doped graphene with concentration of TFSA.

The enhancement of the PLED performance is attributed to reduced sheet resistance and reduced hole-injection barrier from graphene anode to HTL after TFSA doping. Work function is another important factor for anode application to PLEDs. As shown in Figure 5e, the work functions of pristine graphene and 15 mM TFSA-doped graphene were 4.4 and 5.1 eV, respectively. The work function of TFSA-doped graphene was well matched with that of PEDOT:PSS (HTL; Figure 5f). Increased work function of TFSA-doped graphene results in efficient hole injection from the graphene anode to HTL due to decrease of potential barrier between the graphene and the HTL. Therefore, efficiency of PLED fabricated on the TFSA-doped graphene anode is better than that of PLEDs fabricated on a pristine graphene anode.

3. Conclusions

In summary, TFSA-doped graphene was applied as a transparent and flexible electrode for a PLED. The graphene was doped with TFSA by a simple spin-coating process. Compared to previous doping methods, the mentioned method shows some advantages such as negligible decrease of transmittance after doping, smooth surface, stability, and facile process. After TFSA doping, the sheet resistance decreased up to ≈65%, however, decrease of transmittance was negligible. The sheet resistance of the TFSA-doped five-layer graphene with optical transmittance of ≈88% was as low as ≈90 Ω sq^{-1}. The work function of the graphene increased from 4.4 to 5.1 eV after TFSA doping, which resulted in efficient hole injection from the graphene anode to HTL. Therefore, efficiency of PLEDs on the TFSA-doped graphene anode improved compared with that of PLEDs on a pristine graphene anode. Compared with the pristine graphene anode, maximum luminance, maximum current efficiency, and maximum power efficiency were enhanced by 230%, 160%, and 200%, respectively, when the TFSA-doped graphene was applied as the anode. Our demonstration of TFSA-doped graphene as a flexible and transparent electrode of PLED shows that the TFSA-doped graphene electrode could be a promising flexible and transparent electrode.

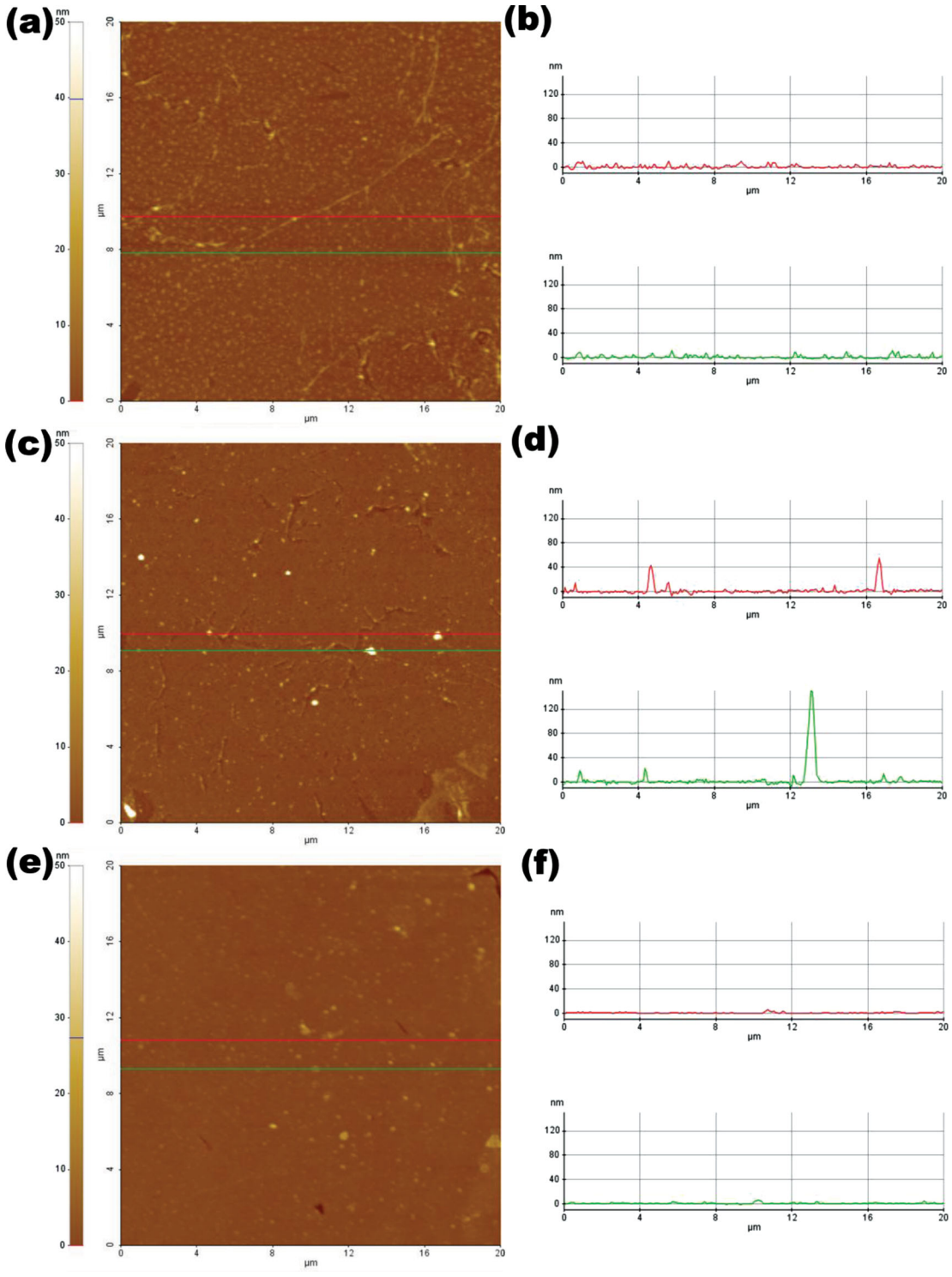

Figure 4. AFM images and line profiles of a,b) pristine graphene, c,d) $AuCl_3$-doped graphene, and e,f) TFSA-doped graphene.

4. Experimental Section

Synthesis of Graphene Samples: Copper foils placed in an inner quartz tube were inserted into a quartz tube and heated at 1000 °C under vacuum for 10 min. Subsequently, evaporation of methanol at a pressure of 10 Torr for 20 min provided a source of carbon atoms. After this process, the copper foils were rapidly cooled to room temperature by removing the samples from the hot zone to room temperature using a magnetic rod. After growth, the graphene grown on copper foil was transferred onto an arbitrary substrate such as a PET or a SiO_2 wafer. by dry transfer. A TRT was applied onto the graphene/copper foil by cold press lamination. After the copper foil had been etched using $FeCl_3$

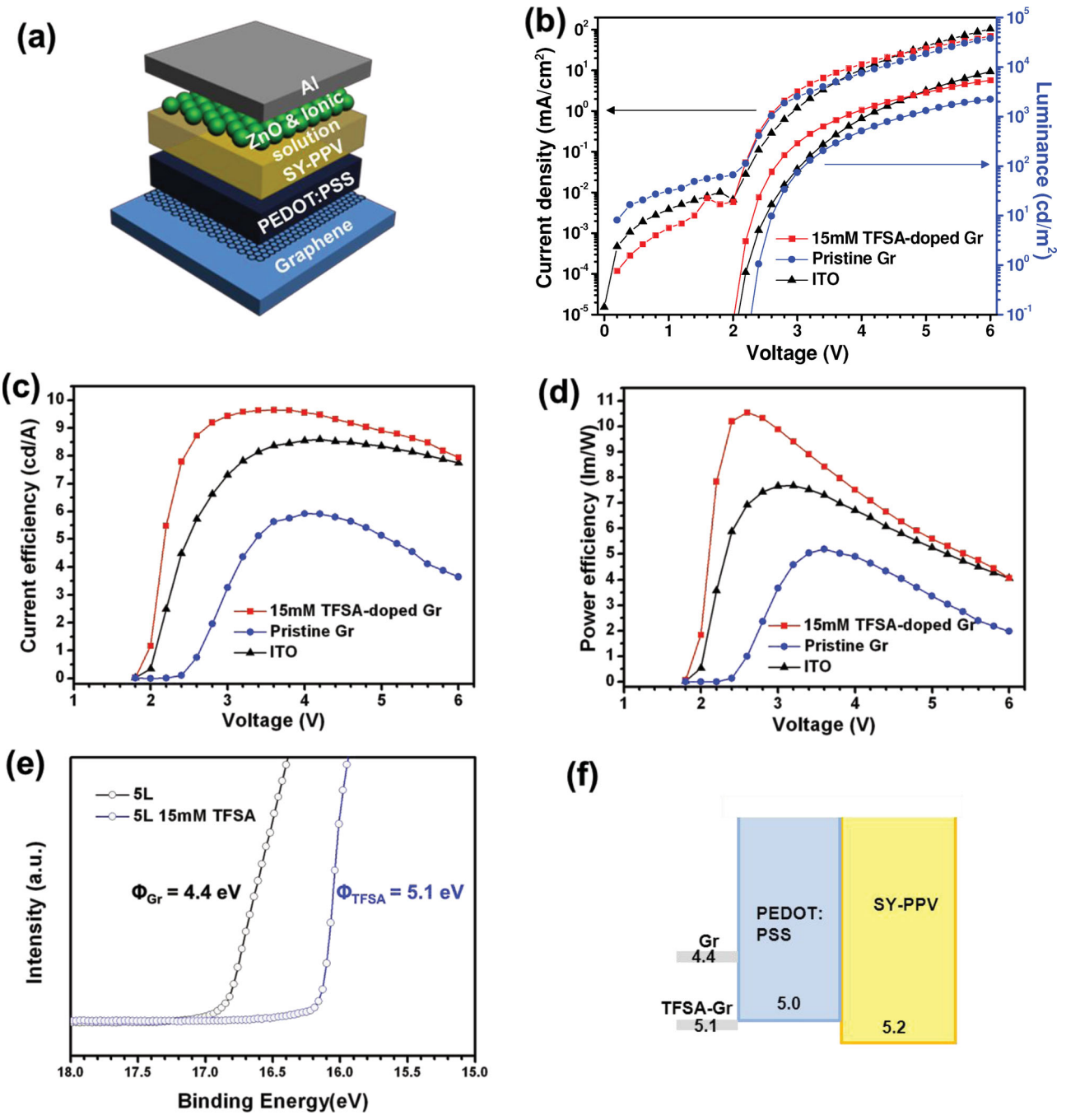

Figure 5. a) Device structure of a flexible PLED fabricated on graphene. b) Current density and luminance vs. voltage characteristics, c) current efficiency vs. voltage characteristics, and d) power efficiency vs. voltage characteristics of flexible PLEDs on pristine five-layer graphene, five-layer graphene doped with 15 mM TFSA, and ITO. e) Ultraviolet photoelectron spectroscopy spectra of pristine five-layer graphene and five-layer graphene doped with 15 mM TFSA. f) Schematic energy diagrams of the PLED.

solution, the graphene attached to the TRT was rinsed with deionized water to remove residual etchant. Subsequently, the graphene was transferred onto an arbitrary substrate such as a PET or a SiO_2 wafer, followed by hot-press lamination. To form multilayered graphene on an arbitrary substrate, this process was repeated until the desired number of graphene layer was obtained.

The graphene samples were doped by a simple spin-coating process. The graphene on the arbitrary substrate was chemically doped with TFSA. TFSA dissolved in nitromethane was spin-coated onto the graphene at 2000 rpm for 1 min (change of sheet resistance of TFSA-doped graphene with time and annealing temperature is shown in Figure S1).

Fabrication of a Flexible PLED: A flexible PLED was fabricated on an ITO (≈10 Ω sq^{-1}, ≈90%), pristine five-layer graphene/PET, or TFSA-doped five-layer graphene/PET substrate by spin-coating.[30] A PEDOT:PSS layer was spin-coated onto the graphene/PET substrate at 2000 rpm for 60 s

Table 1. Light-emitting characteristics of PLEDs fabricated on ITO, pristine five-layer graphene, and TFSA-doped five-layer graphene anodes.

Anode	Max. luminance [cd m^{-2} @ bias]	Max. current efficiency [cd A^{-1} @ bias]	Max. power efficiency [lm W^{-1} @ bias]	Turn-on voltage [V][a)]
ITO[30]	24000@ 9.0	6.3 @ 5.4	–	–
ITO (Our work) (≈10 Ω sq^{-1}, ca. 90%)	8100 @ 6.0	8.6 @ 4.2	7.7 @ 3.2	2.2
5L Pristine Gr (≈240 Ω sq^{-1}, 88%)	2300 @ 6.0	5.9 @ 4.0	5.2 @ 3.6	2.4
5L TFSA-doped Gr (≈90 Ω sq^{-1}, 88%)	5400 @ 6.0	9.6 @ 3.6	10.5 @ 2.6	2.2

[a)]Turn-on voltage is defined at the luminance of 1 cd m^{-2}.

and subsequently the PEDOT:PSS-coated graphene/PET substrate was heated on a hot plate at 140 °C for 30 min. For the emissive layer of the PLED, a commercially available polymer known as "Super Yellow–PPV" (Merck, PDY 132; SY) was dissolved in toluene at a concentration of 5 mg mL^{-1}. On top of the PEDOT:PSS layer, SY solution was spin-coated at 2000 rpm for 60 s, after which it was annealed at 100 °C for 30 min. The ZnO nanoparticle layer and ionic solution (a blend of PEO and $TBABF_4$) were spin-coated and then baked at 50 °C. Finally, a 120-nm thick aluminum layer was deposited by thermal evaporation.

Characterization: Raman spectra were obtained by using a Horiba Jobin Yvon Raman spectrometer (LabRAM HR UV/Vis/NIR at 514 nm). A UV-vis spectrometer (Shimadzu UV-3101 PC spectrometer) was utilized to measure the optical transmittance of the prepared samples. The sheet resistance of the graphene samples was measured by using the van der Pauw method. The AFM images were recorded on a XE-70, Park Systems. The work function of graphene was obtained from ultraviolet photoelectron spectroscopy (Sigma Probe, Thermo VG Scientific). The characteristics of luminance vs. applied voltage were measured using a Keithley 2400 source measurement unit and a Konica Minolta spectroradiometer (CS-2000).

Supporting Information

Supporting Information is available from the Wiley Online Library or from the author.

Acknowledgements

This research was supported by WCU (World Class University) program through the National Research Foundation of Korea (NRF) funded by the Ministry of Education, Science and Technology (R32–10051) and Basic Science Research Program through the National Research Foundation of Korea (NRF) funded by the Ministry of Education (NRF-2012R1A1A2043856).

Received: April 24, 2013
Revised: June 13, 2013
Published online: August 19, 2013

[1] K. S. Novoselov, A. K. Geim, S. V. Morozov, D. Jiang, Y. Zhang, S. V. Dubonos, I. V. Grigorieva, A. A. Firsov, *Science* **2004**, *306*, 666.
[2] Y. Lee, S. Bae, H. Jang, S. Jang, S. E. Zhu, S. H. Sim, Y. I. Song, B. H. Hong, J. H. Ahn, *Nano Lett.* **2010**, *10*, 490.
[3] K. S. Kim, Y. Zhao, H. Jang, S. Y. Lee, J. M. Kim, K. S. Kim, J. H. Ahn, P. Kim, J. Y. Choi, B. H. Hong, *Nature* **2009**, *457*, 706.
[4] S. Bae, H. Kim, Y. Lee, X. F. Xu, J. S. Park, Y. Zheng, J. Balakrishnan, T. Lei, H. R. Kim, Y. I. Song, Y. J. Kim, K. S. Kim, B. Ozyilmaz, J. H. Ahn, B. H. Hong, S. Iijima, *Nat. Nanotechnol.* **2010**, *5*, 574.
[5] Z. G. Wang, Y. F. Chen, P. J. Li, X. Hao, J. B. Liu, R. Huang, Y. R. Li, *ACS Nano* **2011**, *5*, 7149.
[6] T. H. Han, Y. Lee, M. R. Choi, S. H. Woo, S. H. Bae, B. H. Hong, J. H. Ahn, T. W. Lee, *Nat. Photonics* **2012**, *6*, 105.
[7] L. G. De Arco, Y. Zhang, C. W. Schlenker, K. Ryu, M. E. Thompson, C. W. Zhou, *ACS Nano* **2010**, *4*, 2865.
[8] S. Lee, J. S. Yeo, Y. Ji, C. Cho, D. Y. Kim, S. I. Na, B. H. Lee, T. Lee, *Nanotechnology* **2012**, *23*, 344013.
[9] Z. Y. Yin, S. Y. Sun, T. Salim, S. X. Wu, X. A. Huang, Q. Y. He, Y. M. Lam, H. Zhang, *ACS Nano* **2010**, *4*, 5263.
[10] P. Matyba, H. Yamaguchi, M. Chhowalla, N. D. Robinson, L. Edman, *ACS Nano* **2011**, *5*, 574.
[11] A. Das, S. Pisana, B. Chakraborty, S. Piscanec, S. K. Saha, U. V. Waghmare, K. S. Novoselov, H. R. Krishnamurthy, A. K. Geim, A. C. Ferrari, A. K. Sood, *Nat. Nanotechnol.* **2008**, *3*, 210.
[12] Y. J. Yu, Y. Zhao, S. Ryu, L. E. Brus, K. S. Kim, P. Kim, *Nano Lett.* **2009**, *9*, 3430.
[13] D. C. Wei, Y. Q. Liu, Y. Wang, H. L. Zhang, L. P. Huang, G. Yu, *Nano Lett.* **2009**, *9*, 1752.
[14] L. S. Panchokarla, K. S. Subrahmanyam, S. K. Saha, A. Govindaraj, H. R. Krishnamurthy, U. V. Waghmare, C. N. R. Rao, *Adv. Mater.* **2009**, *21*, 4726.
[15] J. O. Hwang, J. S. Park, D. S. Choi, J. Y. Kim, S. H. Lee, K. E. Lee, Y. H. Kim, M. H. Song, S. Yoo, S. O. Kim, *ACS Nano* **2012**, *6*, 159.
[16] H. Medina, Y. C. Lin, D. Obergfell, P. W. Chiu, *Adv. Funct. Mater.* **2011**, *21*, 2687.
[17] W. Chen, S. Chen, D. C. Qi, X. Y. Gao, A. T. S. Wee, *J. Am. Chem. Soc.* **2007**, *129*, 10418.
[18] C. L. Hsu, C. T. Lin, J. H. Huang, C. W. Chu, K. H. Wei, L. J. Li, *ACS Nano* **2012**, *6*, 5031.
[19] H. B. Wang, T. Maiyalagan, X. Wang, *ACS Catal.* **2012**, *2*, 781.
[20] X. C. Dong, D. L. Fu, W. J. Fang, Y. M. Shi, P. Chen, L. J. Li, *Small* **2009**, *5*, 1422.
[21] H. J. Shin, W. M. Choi, D. Choi, G. H. Han, S. M. Yoon, H. K. Park, S. W. Kim, Y. W. Jin, S. Y. Lee, J. M. Kim, J. Y. Choi, Y. H. Lee, *J. Am. Chem. Soc.* **2010**, *132*, 15603.
[22] A. Kasry, M. A. Kuroda, G. J. Martyna, G. S. Tulevski, A. A. Bol, *ACS Nano* **2010**, *4*, 3839.
[23] K. C. Kwon, K. S. Choi, S. Y. Kim, *Adv. Funct. Mater.* **2012**, *22*, 4724.
[24] J. Lee, E. Hwang, E. Lee, S. Seo, H. Lee, *Chem. Eur. J.* **2012**, *18*, 5155.
[25] G. Eda, Y. Y. Lin, S. Miller, C. W. Chen, W. F. Su, M. Chhowalla, *Appl. Phys. Lett.* **2008**, *92*, 233305.
[26] S. M. Kim, Y. W. Jo, K. K. Kim, D. L. Duong, H. J. Shin, J. H. Han, J. Y. Choi, J. Kong, Y. H. Lee, *ACS Nano* **2010**, *4*, 6998.
[27] S. Tongay, K. Berke, M. Lemaitre, Z. Nasrollahi, D. B. Tanner, A. F. Hebard, B. R. Appleton, *Nanotechnology* **2011**, *22*, 425701.
[28] X. C. Miao, S. Tongay, M. K. Petterson, K. Berke, A. G. Rinzler, B. R. Appleton, A. F. Hebard, *Nano Lett.* **2012**, *12*, 2745.
[29] H. Park, J. A. Rowehl, K. K. Kim, V. Bulovic, J. Kong, *Nanotechnology* **2010**, *21*, 505204.
[30] H. Youn, M. Yang, *Appl. Phys. Lett.* **2010**, *97*, 243302.